



# Late Quaternary depositional and glacial history of the Arliss Plateau off the East Siberian margin in the western Arctic Ocean

Young Jin Joe <sup>a, b</sup>, Leonid Polyak <sup>c</sup>, Michael Schreck <sup>a, d</sup>, Frank Niessen <sup>e</sup>, Seok Hoon Yoon <sup>b</sup>, Gee Soo Kong <sup>f</sup>, Seung-Il Nam <sup>a, \*</sup>

<sup>a</sup> Division of Polar Paleoenvironment, Korea Polar Research Institute, 21990, Incheon, Republic of Korea

<sup>b</sup> Department of Earth and Marine Sciences, Jeju National University, 63243, Jeju, Republic of Korea

<sup>c</sup> Byrd Polar and Climate Research Center, The Ohio State University, 1090 Carmack Road, Columbus, OH, 43210, USA

<sup>d</sup> Department of Geosciences, UiT-The Arctic University of Norway, N-9037, Tromsø, Norway

<sup>e</sup> Alfred Wegener Institute (AWI) Helmholtz Centre for Polar and Marine Research, D-27568, Bremerhaven, Germany

<sup>f</sup> Petroleum and Marine Division, Korea Institute of Geoscience and Mineral Resources, 34132, Daejeon, Republic of Korea

## ARTICLE INFO

### Article history:

Received 1 July 2019

Received in revised form

20 November 2019

Accepted 22 November 2019

Available online 5 December 2019

### Keywords:

Arctic Ocean sediments

Late Quaternary

Glacial history

Sediment facies

Seismostratigraphy

## ABSTRACT

Sedimentary stratigraphy and facies analysis along with seismostratigraphic and multibeam bathymetry data are used to reconstruct the last glacial impact on the Arliss Plateau (AP) and attendant sedimentation in the adjacent Chukchi Basin (CB) in the western Arctic Ocean off the East Siberian margin. Sediment core ARA02B/16B-GC from the AP lower slope captures glacier-related depositional history during the last estimated ca. 100 ka (Marine Isotope Stage, MIS 1 to 5c) based on regional lithostratigraphic correlation. The sedimentary record shows distinguishable interglacial (interstadial) and glacial (stadial) patterns. The identified sedimentary facies reflect several modes of glaciogenic deposition by drifting icebergs, suspension settling from turbid meltwater plumes and/or detached underflows, and turbidity currents. Based on strong seismic reflectors related to lithological boundaries, a downslope subbottom profile from AP to CB is divided into seismostratigraphic units (SSU) 1 and 2 corresponding in the core record to MIS 1–3 and MIS 3–5c, respectively. An acoustically transparent lens within SSU 2 correlates on the upper slope to debris lobes downslope from the AP top covered by megascale glacial lineations. This geomorphic/sedimentary pattern indicates a glacial erosional impact on the AP and proglacial deposition of eroded sediments on the slope and in the basin. Based on the developed sediment stratigraphy and facies analysis, the last debris lobe horizon was deposited in glacial/deglacial environments during late MIS 4 to early MIS 3. The absence of similar glaciogenic debris lobes within SSU 1 indicates no direct glacial impact on the AP during the Last Glacial Maximum (LGM). These results suggest that the last glacial erosion of the AP occurred during or immediately after MIS 4, possibly related to major glaciation in northern Siberia at ~50–70 ka.

© 2019 Elsevier Ltd. All rights reserved.

## 1. Introduction

Over last two decades, multiple geophysical investigations along with sedimentary records revealed that the Arctic East Siberian and Chukchi continental margins have been repeatedly glaciated during the Pleistocene (Jakobsson et al., 2008, 2014; Polyak et al., 2007; Niessen et al., 2013; Dove et al., 2014; O'Regan et al., 2017). In particular, streamlined glacial lineations and related diamicton

deposits identified by swath seafloor and subbottom profiling on the East Siberian margin, including the adjacent part of the Mendeleev Ridge known as the Arliss Plateau (AP) (Fig. 1C), indicate the repeated development of up to 1 km-thick marine ice sheets/ice shelves (Niessen et al., 2013). However, the age framework for these glacial events, and thus, their relation to a broader paleoclimatic context, is not well understood. Recently, Schreck et al. (2018) provided lithostratigraphic insight on glacial impacts on the East Siberian margin in the Late Pleistocene, concluding that the last major regional ice grounding occurred during MIS 4 to 3 (60–70 ka). This conclusion differs from the notion that this event was coeval with the deepest glacial erosion on the Lomonosov Ridge in

\* Corresponding author. Division of Polar Paleoenvironment, Korea Polar Research Institute, 21990, Incheon, Republic of Korea.

E-mail address: [sinam@kopri.re.kr](mailto:sinam@kopri.re.kr) (S.-I. Nam).

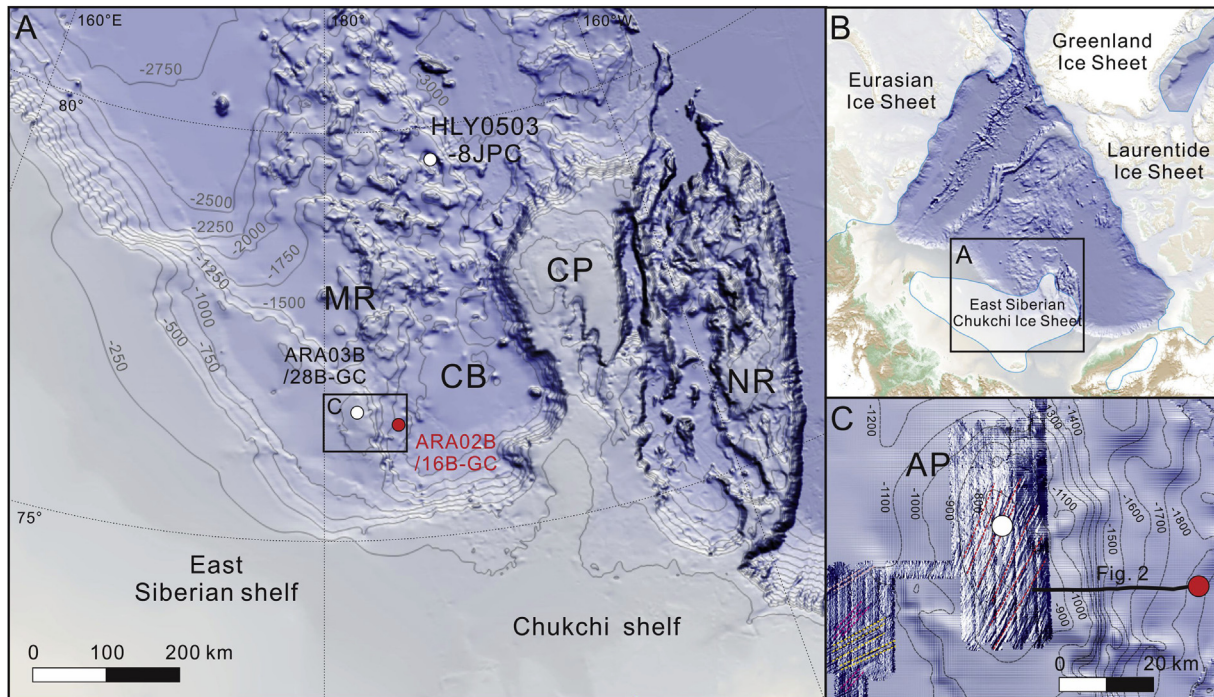


**Fig. 1.** (A) Index physiographic map of the study area showing the location of cores ARA02B/16B-GC (this study), ARA03B/28B-GC (Schreck et al., 2018) and HLY0503-8JPC (Adler et al., 2009). MR, Mendeleev Ridge; AP, Arliss Plateau; CB, Chukchi Basin; CP, Chukchi Plateau; NR, Northwind Ridge. Solid line tracks sub-bottom profiler data. Bathymetric contour interval is 250 m. (B) Broader physiographic/paleogeographic context with inferred ice-sheet maxima shown by semi-transparent white fill (Svendsen et al., 2004; Niessen et al., 2013; Stokes et al., 2016). (C) Multibeam bathymetry of the Arliss Plateau showing several generations of Mega-Scale Glacial Lineations. Bathymetric contour interval is 100 m.

the central Arctic Ocean (Jakobsson et al., 2016; O'Regan et al., 2017), which has been constrained to MIS 6 (Jakobsson et al., 2001).

To better constrain the timing of ice grounding events and their spatial pattern, it is important to link the geophysical records and sediment core stratigraphy. This task requires analyzing representative sedimentary records accompanied by sub-bottom seismic profiles and detailed multibeam bathymetry from the areas affected by glaciations. However, most areas of continental margins, as well as bathymetric highs on the oceanic ridges and plateaus impacted by glacial erosion or iceberg turbation, are unsuitable for recovering well preserved, stratigraphically coherent records (Polyak et al., 2007; Jakobsson et al., 2008; Dove et al., 2014). In comparison, the adjacent slopes and basins may hold more expanded, better-preserved stratigraphies, provided their depositional context, which is sufficiently constrained by geophysical data. In particular, the slope of the AP and the adjacent Chukchi Basin (CB) were chosen for this study as a relatively well surveyed area of deposition for glaciogenic material originating from the East Siberian continental margin (Niessen et al., 2013; Jakobsson et al., 2014; Schreck et al., 2018). We are using a sediment core collected on a CHIRP sub-bottom profile (SBP) from the AP top to the CB (Fig. 1) to reconstruct the depositional history of the East Siberian margin during and since the last glacial grounding event.

## 2. Regional setting

### 2.1. Seafloor morphology and sedimentary cover

The CB is bounded by the Mendeleev Ridge/AP and the Chukchi Plateau and shelf and is connected to the north with the Canada Basin (Fig. 1). The CB covers ~43,000 km<sup>2</sup> (Jakobsson et al., 2003) and has a relatively flat and smooth seafloor ranging from 1800 to 2300 m water depth and comprised of well-stratified deposits

(Dove et al., 2014). The tops of both the Arliss and the Chukchi plateaus are covered by streamlined morphological features interpreted as megascale glacial lineations (MSGL), complicated in some areas with transverse ridges (Niessen et al., 2013; Dove et al., 2014; Jakobsson et al., 2014, 2016). The outer parts of the East Siberian and Chukchi margins at water depths to 700 m feature extensive till wedges and recessional moraines related to repeated glacial advances and retreats (Niessen et al., 2013; Dove et al., 2014; Jakobsson et al., 2014). Further downslope these margins as well as adjacent borderlands, including the AP, hold large, lens-shaped debris lobes (Fig. 2), similar to seismostratigraphic features observed in the glacial trough mouth fans in front of large ice streams (Batchelor and Dowdeswell, 2014; Jakobsson et al., 2014; O'Regan et al., 2017).

### 2.2. Sediment stratigraphy in the western Arctic Ocean

The Quaternary western Arctic sediments are generally characterized by the cyclical pattern of dark brownish and olive/greyish units (Phillips and Grantz, 1997; Polyak et al., 2004, 2009; Adler et al., 2009; Stein et al., 2010; Schreck et al., 2018). This color contrast was shown to be controlled by the content of manganese (Mn) (oxy)hydroxides, with higher values in brown units attributed to Mn inputs from the continental margins at higher sea levels during interglacial/major interstadial periods (Jakobsson et al., 2000; Polyak et al., 2004, 2009; März et al., 2011; Löwemark et al., 2014; Ye et al., 2019). While Mn-enriched intervals can be affected by diagenetic remobilization and redistribution of this redox-sensitive element, their stratigraphic pattern is consistent throughout the central Arctic Ocean (März et al., 2011; Löwemark et al., 2014; Schreck et al., 2018). Their correlation is corroborated in multiple cores by the distribution of other lithostratigraphic parameters, such as sediment density, ice-rafted debris (IRD), and

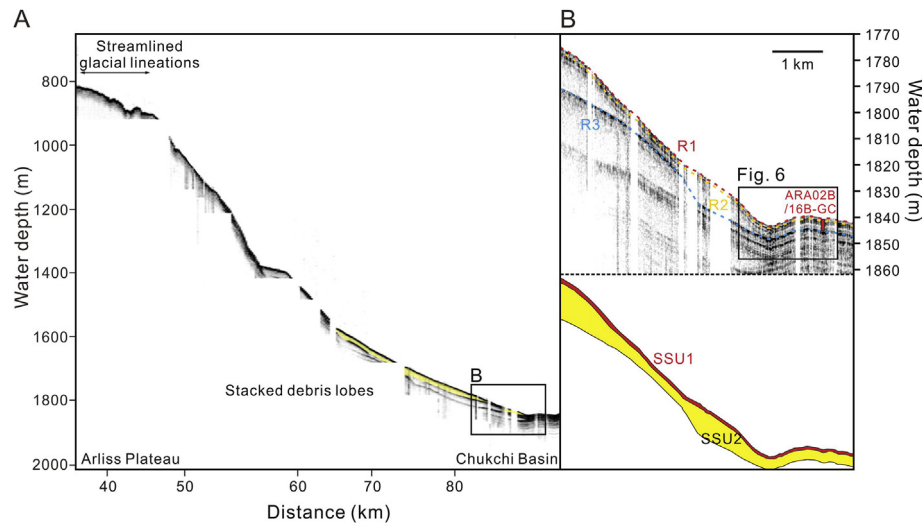


**Fig. 2.** Sub-bottom profile from Arliss Plateau to Chukchi Basin across the site of core ARA02B/16B-GC (red vertical bar in panel B). Seismostratigraphic units, SSUs 1 and 2 are bounded by distinct reflectors R1 to 3. The uppermost glaciogenic debris lobes on the slope are correlated with the lower part of SSU 2. Black box in Fig. 2B shows the position of Fig. 6.

biogenic proxies. The brown, Mn-enriched units (layers), interpreted as interglacial/major interstadial sedimentary intervals, are typically characterized also by low to moderate amounts of coarse IRD, intense bioturbation, and relatively abundant microfossils (Polyak et al., 2004, 2009; Adler et al., 2009; Stein et al., 2010; Löwemark et al., 2012). In comparison, olive/greyish, Mn-depleted units, related to glacial periods, are composed of fossil-poor sediments with strongly variable IRD amounts (Polyak et al., 2004, 2009; Adler et al., 2009; Stein et al., 2010). Fine-grained and IRD-rich lithological types of grey sediments have been attributed to glacial maxima and deglacial depositional environments, respectively. At sites proximal to glaciated areas, deglacial sediments may have expanded thicknesses indicative of high depositional rates (Polyak et al., 2007; Wang et al., 2013; Schreck et al., 2018). Some of the IRD peaks have characteristic sediment compositions used as provenance indicators. In particular, detrital carbonates (mostly dolomites) are related to the Paleozoic platform of the Canadian Arctic eroded by the Laurentide Ice Sheet (LIS) (Bischof and Darby, 1997; England et al., 2009; Polyak et al., 2009; Stein et al., 2010; Bazhenova et al., 2017; Dong et al., 2017). Peaks of this material forming characteristic pinkish-white (PW) layers in sediment cores (Clark et al., 1980) can be used to track the distribution of icebergs in the Arctic Ocean during the LIS collapse events.

### 3. Material and methods

#### 3.1. Material

We use a 378-cm-long, 12-cm in diameter gravity sediment core ARA02B/16B-GC (hereafter 16B-GC) and high frequency (2.5–6.5 kHz) subbottom CHIRP profile collected on the AP slope (Fig. 1) during the 2<sup>nd</sup> RV *Araon* Arctic Expedition (ARA02B) in 2011. Multibeam bathymetry mapping of the AP top (Fig. 1C) was subsequently conducted in 2012 (ARA03B). The 16B coring site (76° 24' N, 175° 58' W, 1841 meter water depth (mwd)) was selected based on the AWI Parasound data acquired previously on the 2008 RV *Polarstern* Arctic expedition ARK-24/3 (Jokat, 2008). The site is located ~1 km downslope from the foot of glaciogenic debris lobes and features relatively flat and smooth seafloor with acoustically well stratified subbottom reflectors (Fig. 2). A 38-cm-long box core 16B-BC was taken at the same site to recover the surficial sediment.

Based on the comparison with 16B-BC, about 10 cm of top sediment is lost in 16B-GC, including the surficial brown lithological unit B1, which was spliced for a composite record of 16B-BC (Figs. 3 and 4).

#### 3.2. Methods

After a visual description of the split core, its line-scan images and elemental geochemistry were acquired with AVAATECH XRF-core scanner at Korea Institute of Geoscience and Mineral Resources (KIGAM). Line-scanning was conducted using a Jai CV L107 camera with red-green-blue (RGB) channels. L\* (lightness) and a\* (red-green color space) data were used for correlation with previously published sediment records (Schreck et al., 2018). Sediment elemental composition was measured at 5-mm intervals using X-ray fluorescence (XRF) AVAATECH scanner settings reported in Schreck et al. (2018). Mn and calcium (Ca) XRF data used in lithostratigraphic correlation were normalized to aluminum (Al) to eliminate the potential dilution effect of background sedimentation (e.g., März et al., 2011). We note, however, that Mn and Ca variations in Arctic sediments are largely independent of the background lithogenic elements as shown in prior studies (e.g., Löwemark et al., 2014; Dong et al., 2017).

X-radiographs were performed for detailed sediment structure on 1 × 10 × 30 cm slabs. X-ray images were taken with SOFTEX m-100w digital x-ray scanner (EZ-320) and instantly processed using iX-Pect X-Ray imaging software. Darker objects in X-radiographs presented in this study display dense material, such as lithic fragments. Coarse debris >2 mm in diameter was counted at every 1 cm, according to Grobe (1987). Samples for sediment texture were taken at 10 cm intervals and treated with 35% H<sub>2</sub>O<sub>2</sub> to decompose organic matter. Sand-sized and coarser grains were separated by wet sieving at 63 μm and dry sieving at 2 mm standard sieves. The grain size of <63-μm sediment was measured with a Micromeritics Sedigraph 5000D.

The multibeam bathymetric survey was performed using a hull-mounted EM122 echosounder. Acquired bathymetric data were processed onboard using a specialized software CARIS. Sub-bottom seismic-reflection data were acquired with the CHIRP SBP-120 profiler with the vertical resolution on the 10 cm scale in acoustically stratified sediments. The SBP data were logged in the TOPAS raw format, which was converted to an SEG-Y format and allowed

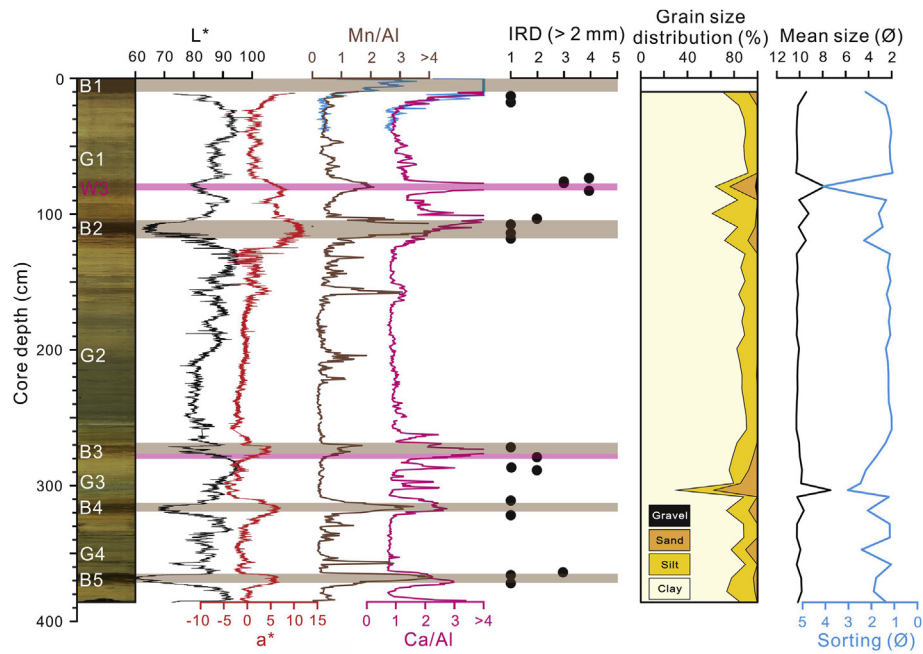


**Fig. 3.** Down-core distribution of sediment lightness ( $L^*$ ), red-green color space ( $a^*$ ), Mn/Al and Ca/Al ratios, IRD numbers, and grain size in core ARA02B/16B-GC. Top 10 cm are estimated to be missing due to overpenetration; XRF data for this interval (blue-colored solid lines) are spliced from the box core 16B-BC. High Mn/Al and Ca/Al ratios in surficial sediment may be partially due to high water content (Thallinghii et al., 2007).

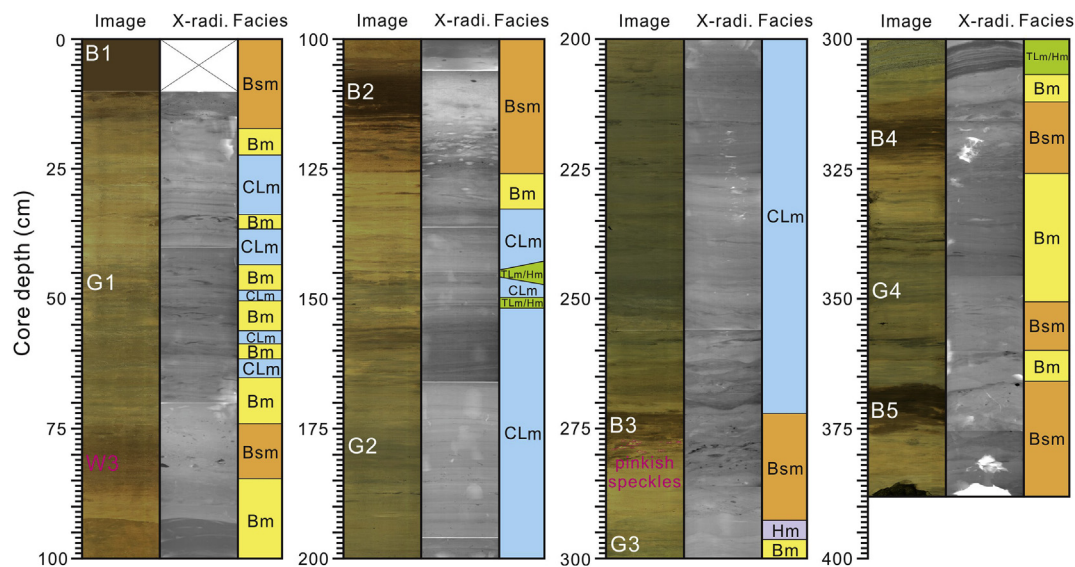


**Fig. 4.** Split-core photos, X-radiograph images, and sedimentary facies (see Table 1 for details). Indices for lithological units (B1–B5 and G1–G4) and the detrital carbonate layer W3 are shown on the core photo.

for post-processing with standard software packages. The estimated sound velocity of 1500 m/s was used to convert the signal travel time into sediment depth for comparison with core lithostratigraphy.

## 4. Results

### 4.1. Lithostratigraphy

Core 16B-GC is composed of sandy to fine-grained mud displaying a general cyclic depositional pattern characterized by an

alternation of brown to dark brown and yellow to olive greyish sedimentary units (Figs. 3 and 4). The concentration of coarse IRD (>2 mm) increases at lithological boundaries and within some brown units, whereas IRD within yellow to olive greyish units is typically rare.

A total of five Mn-rich brown units, B1 to B5, are identified in the recovered stratigraphy based on sediment color, and Mn/Al ratio (Fig. 3) along with sedimentary structure and texture (Fig. 4), including the upper unit B1 spliced from the box core 16B-BC. The brown units show a characteristic low- $L^*$  (darker) and high- $a^*$  (more reddish) color pattern with a relatively symmetrical

distribution across each unit (Fig. 3). High Mn/Al ratios in surficial sediments may be partially due to high water content (Tjallingii et al., 2007), but that does not affect the stratigraphic distribution of Mn values, which are high in unit B1. The brown units mostly consist of slightly sandy mud with scattered IRD and have relatively sharp upper boundary and uneven, bioturbated (mottled) lower boundary (Fig. 4). Yellowish to olive-grey units are generally thicker than brown units and are mostly composed of fine-grained mud without coarse IRD. In particular, the second grey unit between B2 and B3 is the thickest interval recovered (~150 cm) with a consistent lithology. Two PW carbonate layers, consisting of sandy-gravelly mud and expressed as relatively solid lenses and adjacent scattered speckles, are identified above B2 and at the base of B3, corresponding to prominent Ca/Al peaks (Figs. 3 and 4).

#### 4.2. Sediment facies

Sediment of core 16B-GC was classified into five major facies based on sedimentary structure, texture, and color (Fig. 4, Table 1): bioturbated sandy mud (Bsm), bioturbated mud (Bm), crudely laminated or layered mud (CLm), thinly laminated mud/muddy sand (TLm/TLs), and homogeneous mud (Hm).

Bioturbated sandy mud (Bsm) is mostly identified in brown



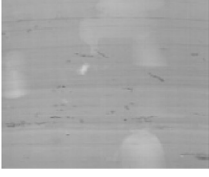
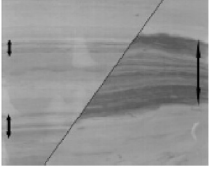

units and PW carbonaceous layers and is characterized by strong bioturbation overprinting primary sedimentary structures, sharp upper- and uneven, mottled lower-boundaries (Fig. 4). This facies mainly consists of very poorly sorted (2–4  $\Phi$ ) sandy mud with coarse particles randomly scattered within the fine matrix (Fig. 3). In comparison with the brown units, Bsm in the PW layers contains higher sand content, up to 22% (Fig. 3), and more coarse particles.

Bioturbated mud (Bm) generally occurs at the transitions between brown and olive-grey units and is characteristic for the olive-grey units underlying B1, where Bm is interbedded with the crudely laminated or layered mud facies (CLm), and below B3 (Fig. 4). Similar to Bsm, the Bm facies also has a mottled structure but is composed of more fine-grained muds with gradual facies boundaries. The sediment sorting index in this facies (1–1.5  $\Phi$ ) is lower than in Bsm due to a lack of coarse particles (Figs. 3 and 4).

Crudely laminated or layered mud (CLm) is characterized by the alternation of planar to sub-parallel silt- and clay-rich laminae or layers with weak bioturbation (Fig. 4). Individual laminae are generally difficult to discern. Clayey laminae/layers are mostly thicker (4–12 mm) than their silt-rich counterparts (1–3 mm). Vertical changes in lamina thickness and composition appear to be random, and the sediment is overall weakly sorted (1–1.5  $\Phi$ ). Facies CLm is predominant within the second olive-grey unit bounded by

**Table 1**

Summary of sedimentary facies in core ARA02B/16B-GC. Black arrows indicate the intervals of TLm, TLs, and Hm facies. See Fig. 4 for the stratigraphic distribution of sedimentary facies.

Facies	Description	Depositional process
Bioturbated sandy mud (Bsm)	 Brown to dark brown and pinkish: (gravelly) sandy mud. IRD- rich; very poorly sorted; intensely bioturbated, absence of primary structure; relatively sharp and flat upper boundaries and mottled lower basal contact	Hemipelagic settling affected by drifting ice (iceberg/sea-ice)
Bioturbated mud (Bm)	 Yellow to olive grey; fine-grained mud, IRD is rare or absent; poorly sorted; located near brown and pinkish layers, repeatedly alternated with poorly defined laminated facies; gradual facies boundaries	Hemipelagic settling
Crudely laminated or layered mud (CLm)	 Yellow to olive grey; silty mud to clayey mud, IRD is absent; poorly sorted; weakly bioturbated, planar and sub-parallel lamina or layers, lamination is laterally discontinuous and poorly defined, clayey lamina or layer is thicker (4–12 mm) than silty lamina (1–3 mm), non-systematic vertical changes, gradual facies boundaries	Repeated settling of suspension from turbid melt water plumes and or detached turbid layers
Thinly laminated mud/sand (TLm/TLs)	 Olive grey; silt-rich mud/sandy mud; IRD is absent, distinct and laterally continuous laminae are coupled with homogenous muds, relatively regular lamina thickness (1–3 mm), sharp lower boundaries and gradational upper boundaries	Bottom-hugging turbidity current
Homogeneous mud (Hm)	 Olive grey, fine-grained mud, IRD is absent; poorly sorted; absence of primary structure as well as any grading and bioturbation; generally coupled with TLm/TLs facies	Rapid settling from fine-grained suspension plumes in the weakening stage of turbidity current

B2 and B3 and is also interbedded with the Bm facies in the first olive-grey unit.

Thinly laminated mud/muddy sand facies (TLM/TLs) can be subdivided into silt-rich mud (TLM) and muddy sand (TLs). This distinct facies has a laterally continuous lamination (a few millimeters thick), typically identified as couplets with overlying homogeneous mud facies (Hm) (Fig. 4). TLM/TLs laminae show sharp lower and gradational upper boundaries, and relatively regular thicknesses (Fig. 3). TLM/TLs facies occur episodically in the second and third olive-grey intervals, between B2 – B3 and B3 – B4, respectively (Figs. 3 and 4).

Homogeneous mud facies (Hm) consists of fine-grained mud characterized by an overall absence of primary structures, bioturbation, or any grading. This facies is mostly interbedded with the thinly laminated facies TLM/TLs on millimeter scales as couplets. Independently occurring Hm facies (3 cm thick) is identified only in the upper part of the third olive-grey interval below B3 (Fig. 4).

#### 4.3. Geomorphology and seismostratigraphy of the AP basinward slope

The seafloor of the AP top shows several sets of streamlined morphological features (Fig. 1C) interpreted in prior studies as megascale glacial lineations (Niessen et al., 2013; Jakobsson et al., 2016). The youngest set of lineations of SSW-NNE orientation is traced to water depths of ~950 m in the southern part of AP, compared to somewhat shallower depths of 850 m in the northern part. The lineated surface is covered by ~3 m thick, acoustically stratified sediment (Niessen et al., 2013).

The subbottom data from the basin-ward middle to the lower slope of the AP (~1600–1800 mwd) show stacked series of debris lobes of ~10–20 km long and up to 25 m thick (Fig. 2A). The debris deposits are covered by acoustically stratified sediments (Figs. 2B and C). Three distinct acoustic reflectors (R1 – R3) were identified by lateral continuity and strong reflectivity. The reflectors divide the upper part of the sediment cover into two major seismostratigraphic units, SSUs 1 and 2.

The surficial unit SSU 1 bounded by reflectors R1 (seafloor) and R2 is laterally continuous and has bedding parallel to R2 (Fig. 2B and C). SSU 1 is characterized by transparent to slightly fuzzy subbottom echoes, with a laterally discontinuous, weak reflector also recognized within this unit (Fig. 2B). SSU 1 thins out from the core 16B site towards the steep middle slope (Fig. 2B and C) and is indistinguishable further up-slope near the AP top.

As seen on records from the basin and lower slope (Fig. 2B), the underlying unit SSU 2, bounded by R2 and R3, is generally characterized by parallel lamination with variable amplitudes and transparent acoustic signature in the middle part of the unit. Further up-slope, two coeval debris lobes are recognized in the lower part of SSU 2, covered by acoustically stratified sediment comprised of the remaining part of SSU 2 and overlying SSU 1 (Fig. 2B and C). Two thin reflectors with low to moderate reflectivity are identified in the lowermost part of SSU 2 in the basin, but cannot be found near the debris lobes on the upper slope (Fig. 2B).

## 5. Discussion

### 5.1. Age model

As core 16B-GC lacks calcareous material for  $^{14}\text{C}$  dating, its age model is constrained by lithostratigraphic correlation with the earlier investigated core ARA03B/28B-GC from the AP top (Schreck et al., 2018) and core HLY0503-8JPC from the foot of the Mendeleev Ridge ~350 km north (Adler et al., 2009). The latter core record has the best regional age control constrained by multiple  $^{14}\text{C}$  datings in

the upper part of the stratigraphy (MIS 1 to 3, units B1–B3),  $^{14}\text{C}$ -calibrated amino-acid racemization (AAR) rates extending to MIS 5 (Kaufman et al., 2008; Adler et al., 2009), and coccolith occurrences (Backman et al., 2009). The correlation is primarily based on sediment color and distribution of Mn and Ca content showing a regionally consistent pattern (Fig. 5) (Polyak et al., 2009; Stein et al., 2010; Schreck et al., 2018). According to  $^{14}\text{C}$  dating, brown, Mn-rich units B1 and B2, including the detrital carbonate layer W3, represent MIS 1 (~9 ka) and MIS 3 (34–45 ka) interglacial/interstadial environments, respectively (Fig. 5; Table 2). The intermittent grey unit G1 thus corresponds to the last glaciation/deglaciation (MIS 2 to 1) and the youngest, pre-glacial part of MIS 3.

Brown units B3 to B5 recovered by core 16B-GC have been attributed in the reference cores to pre-MIS 3 interstadials ranging to MIS 5c, with some variance. Based on coccolith distribution in HLY0503-8JPC, Backman et al., (2009) suggested that B5 represents MIS 5a, while Adler et al. (2009) assigned its age to MIS 5c, consistent with AAR ages (Kaufman et al., 2008). This age model was also used by Schreck et al. (2018), who pointed out that the coccolith stratigraphy cannot pinpoint a specific time interval within MIS 5. In any case, core 16B-GC does not reach the prominent detrital carbonate layer PW2 identified in multiple cores across the western Arctic Ocean, including HLY0503-8JPC (Fig. 5), and attributed to MIS 5d (e.g., Stein et al., 2010; Bazhenova et al., 2017; Dong et al., 2017). Overall, we consider MIS 5c, with the approximate age of ca. 100 ka, as a reasonable estimate for the bottom of 16B-GC.

The developed lithostratigraphic framework indicates that a ~150 cm thick grey unit G2 pre-dates the MIS 3 interstadial, likely being contained in the time interval from MIS 4 to early MIS 3. This prominent lithostratigraphic unit can be traced in multiple cores from the Siberian margin to the Arctic Ocean interior (e.g., Spielhagen et al., 2004; Polyak et al., 2009; Dong et al., 2017; Wang et al., 2018), and has been proposed to correlate to the last pre-LGM glaciation in northern Eurasia with a glacial maximum around 50–60 ka (Svendsen et al., 2004).

In comparison to this, regionally consistent age model, the B2 unit in a very similar nearby record was assigned to MIS 5 based solely on the presence of rare coccoliths, including *E. huxleyi* (core SWERUS-L2-13 PC; <https://bolin.su.se/data/swerus/physical.php>; Fig. 1) (Jakobsson et al., 2016). The occurrence of *E. huxleyi* clearly indicates that the sediments of this unit are younger than MIS 8/7 (Thierstein et al., 1977; Backman et al., 2009). However, due to an overall limited occurrence of coccoliths, *E. huxleyi* presence may not be used to identify specific substages within MIS 5 as attempted previously (e.g., Jakobsson et al., 2001; Spielhagen et al., 2004) because this species can potentially occur in other relatively warm intervals of Arctic sediments. In particular, MIS 3 is a very pronounced interstadial unit in Arctic paleoceanographic records, as exemplified by a high content of Mn and high productivity indicated by abundant planktic and benthic microfossils (Nørgaard-Pedersen et al., 1998; Adler et al., 2009; Hanslik et al., 2010; Schreck et al., 2018). Some authors further inferred reduced sea ice and enhanced the advection of Atlantic waters during this time (Cronin et al., 2012; Poirier et al., 2012). We note that in another SWERUS core from the Siberian margin further west, *E. huxleyi* was also found in B2 with a  $^{14}\text{C}$  age of 33 ka just a little above this finding (O'Regan et al., 2017).

### 5.2. Core-seismic correlation

Distinct acoustic reflectors on seismic records can be formed by vertical changes in acoustic impedance controlled by sediment density and p-wave velocity. Deep-sea Arctic Ocean sediments generally consist of relatively soft fine-grained muds, which are

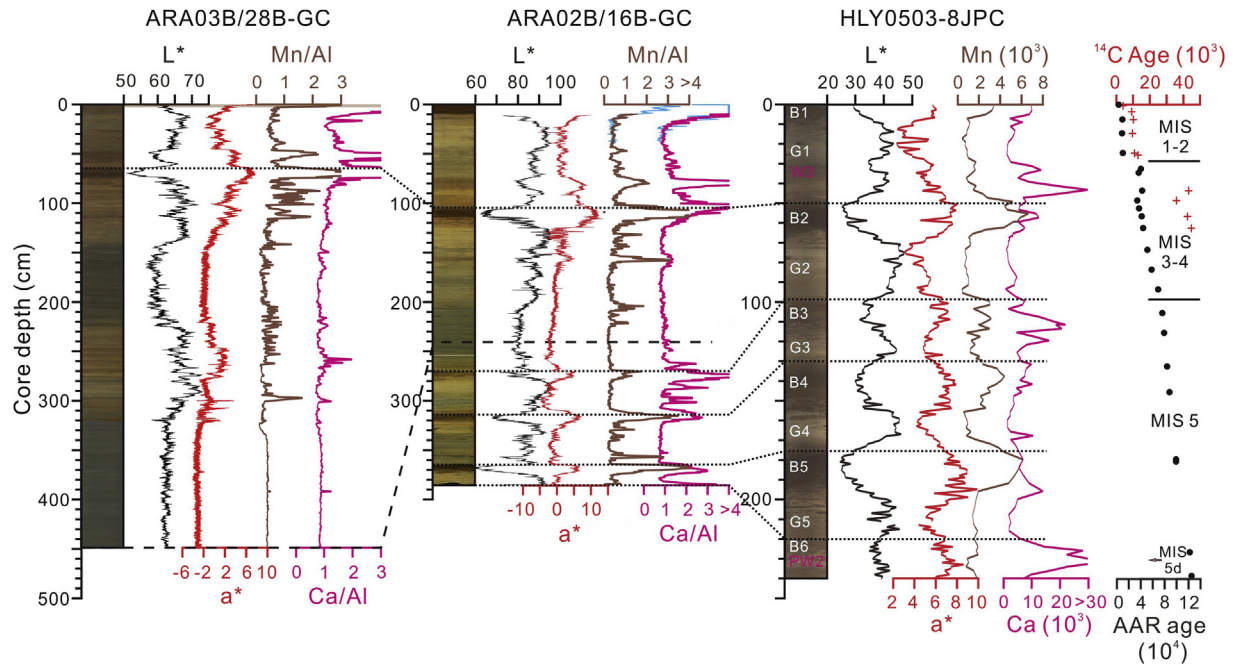


**Fig. 5.** Lithostratigraphic correlation of core ARA02B/16B-GC with ARA03B/28B-GC (Schreck et al., 2018) and HLY0503-8JPC (Adler et al., 2009) based on sediment color and variations of Mn/Al and Ca/Al. The tops of major brown units (B2–B5) are correlated by dotted lines; the bottom of core ARA03B/28B-GC is projected onto ARA02B/16B-GC by the dashed line. Estimated Marine Isotope Stages and radiocarbon/AAR ages (Adler et al., 2009) are shown next to core HLY0503-8JPC.

**Table 2**

Estimated duration and sedimentation rates of lithostratigraphic units in core ARA02B/16B-GC based on the age model developed from lithostratigraphic correlations (Fig. 5).

Lithostratigraphy	Thickness (cm)	Duration (kyr)	Sedimentation Rate (cm/kyr)
B1	10 (0–10)	9 (0–9)	0.83
G1	68 (10–78)	25 (9–34)	2.72
W3–B2	37 (78–115)	11 (34–45)	3.36
G2	157 (115–272)	26 (45–71)	6.04
B3–B5	103 (272–375)	25 (71–96)	4.12

occasionally intercalated with denser, coarse sediment layers mostly attributed to iceberg sedimentation during deglacial events (Clark et al., 1980; Polyak et al., 2009; Stein et al., 2010; Dong et al., 2017; Schreck et al., 2018). In particular, detrital carbonate IRD layers, such as W3 and PW2 captured by western Arctic Ocean sediments, are characterized in cores from the study region by a remarkably high density and p-wave velocity compared to the enclosing fine-grained muds (Matthiessen et al., 2010; Stein et al., 2010; Schreck et al., 2018). These layers, marking the LIS iceberg discharge from the Canadian Arctic, thus have the potential to form strong reflectors.

Comparison of the subbottom acoustic reflection data and core 16B-GC record (Fig. 6) confirms that the surficial reflector R1 represents the seafloor, the interface between bottom water and relatively dense surficial sediment of unit B1. A fine-grained unit G1 characterized by a relatively constant density and p-wave velocity in multiple records from the study region (Matthiessen et al., 2010; Stein et al., 2010; Schreck et al., 2018) defines a mostly transparent echo characteristic of SSU 1. A strong reflector R2 probably indicates a pronounced lithological change from the IRD-rich interval, including the W3 layer to the overlying fine-grained unit G1 (Fig. 6). A relatively strong reflector in the uppermost part of SSU 2, partially divided into two layers, appears to be associated with a relatively coarse unit B2 (Fig. 6). A transparent echo signature similar to that

in SSU 1 characterizes the upper part of SSU 2 corresponding to the fine-grained, thickest unit G2. Two thin reflectors of low to moderate amplitude in the lower part of SSU 2 appear to correspond to a relatively sandy unit B3, especially its detrital carbonate-rich base layer, and an intermittent sandy layer within G3 (Fig. 6). While core 16B-GC does not extend to the depth of R3, a likely candidate for this strong reflector is a prominent, IRD-rich, detrital carbonate layer PW2 that underlies unit B6 and is barely reached by 16B-GC (Fig. 5). PW2 is characterized by a significantly higher wet bulk density and p-wave velocity than other Upper Quaternary sediments in the study region (Matthiessen et al., 2010; Schreck et al., 2018).

### 5.3. Glaciogenic debris lobes on the AP slope

The presence of debris lobes in the lower part of SSU 2 up-slope from core 16B-GC (Fig. 2) is likely related to glacial scouring on the AP crest. While debris flows can potentially originate from various slope instability processes, the consistent occurrence of these lobes in the Arctic Ocean downslope from continental margins and plateaus characterized by glacial erosion/deposition indicates their glaciogenic origin. In particular, the CB features debris lobes on both the AP and Chukchi Plateau slopes (Niessen et al., 2013; Dove et al., 2014 and reference therein), indicating glaciogenic inputs from

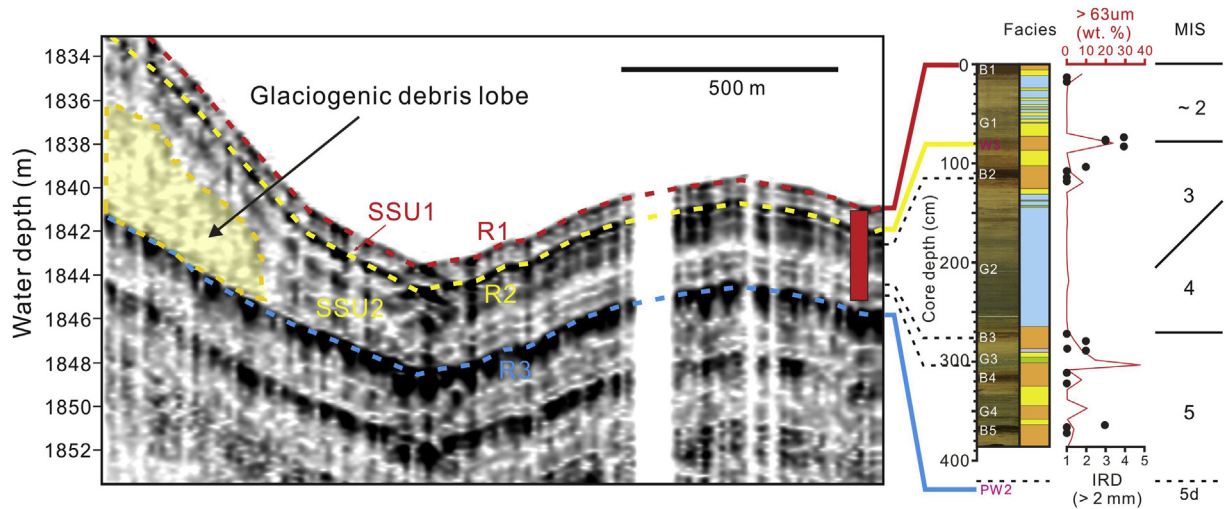


**Fig. 6.** Correlation of the subbottom data with core ARA02B/16B-GC. Surficial reflector R1 is the seafloor. Strong reflectors R2 and R3 correspond to prominent lithological changes at the boundaries of fine-grained sediments and IRD-rich layers W3 and PW2. Estimated Marine Isotope Stages are shown on the right.

both sides. The mechanisms for debris flows could include sediment bulldozing on the tops by grounded ice and/or rapid deposition of deglacial sediments, e.g., from glacial underflows (e.g., Powell, 1990; Batchelor and Dowdeswell, 2015). The timing of debris lobe emplacement would thus correspond to glacial advance or early deglaciation stages.

The SSW-NNE orientation and southward inclination of the youngest set of glacial lineations on the AP top indicate that the eroding ice was sourced from the East Siberian margin (Niessen et al., 2013). According to the age constraints developed for core 16B-GC and a correlative core 28B-GC from the AP top (Fig. 5), this event occurred prior to the MIS 3 interstadial and was possibly related to a major glaciation in northern Siberia dated to the time interval between ~70 and 50 ka (Svendsen et al., 2004; Möller et al., 2015).

The upper seismostratigraphic unit SSU 1 bounded by the seafloor, and the W3 layer represents deposition during the time interval from late MIS 3 to the Holocene (Fig. 6). The absence of glaciogenic debris lobes within SSU 1 indicates that glacial erosion of the AP was unlikely during the LGM, as suggested in previous studies (Niessen et al., 2013; Schreck et al., 2018).

#### 5.4. Glacier-induced depositional environments

Based on the developed age model, sedimentary unit G2 (MIS 4 to early MIS 3) that is characterized by laminated mud facies, has a relatively high sedimentation rate of ~6 cm/kyr as compared to more bioturbated units G3 and G4 (Fig. 4, Table 2). Laminated structures of glaciogenic sediments in the high-latitude oceans can be potentially formed under various depositional settings such as permanent sea ice, turbid meltwater plumes, distal fine-grained turbidity currents, and contour currents (Hesse et al., 1996; Darby et al., 1997; Kleiber et al., 2000; ÓCofaigh et al., 2003; Matthiessen et al., 2010). However, contour currents are unlikely to be strong in a semi-enclosed Arctic deep-sea basin, while sedimentation rates under perennial sea ice are too low to form a laminated sedimentary sequence. Couplets of TLM/TLs and Hm facies similar to those observed in 16B-GC (Fig. 4) have been interpreted in previous studies as deposition from underflow turbidity currents in combination with rapid settling from fine-grained suspension plumes in the attenuation stage of the carrying current (Piper, 1978; Chough, 1984; Yoon et al., 1991). The

occurrence of TLM/TLs facies within G2 and G3 suggests that turbidities could be associated with the glaciogenic debris flows emanating from their front on a relatively steep AP slope (Fig. 2B). The development of CLm facies may reflect deposition from turbid meltwater plumes repeatedly discharged from ice-sheet termini (Hesse et al., 1996; Kleiber et al., 2000; ÓCofaigh et al., 2003).

Glacial erosion on glaciated continental margins plays an important role in delivering large amounts of sediments to the continental slope and the adjacent basins, and thus leading to the formation of debris flows (Vorren et al., 1998; Kleiber et al., 2000; Dowdeswell and Elverhøi, 2002; Jakobsson et al., 2008). Based on our seismostratigraphic and sediment core data, this scenario applies to the AP during MIS 4, when large volumes of eroded sediment may have been transported as proglacial under- and overflows into the adjacent deep basin. This rapid sediment deposition likely caused slope instability and thus triggered debris flows. Suspended fine sediments could have been detached from the slope and transported into the interior of the Arctic Ocean at the density boundaries between different water masses with subsequent deposition. Prolonged glacial erosion could have also formed repeatedly detached turbid layers, leading to the formation of crudely laminated mud (CLm) facies (Fig. 7A). As the grounded ice retreated, turbid meltwater underflow plumes were likely repeatedly discharged from the grounding line, thereby depositing CLm facies (Hesse et al., 1996; ÓCofaigh et al., 2003) (Fig. 7B). These glacier-induced processes could lead to the deposition of fine-grained, fully laminated sediments with fairly high sedimentation rates (unit G2) during the MIS 4 deglaciation that may have extended to early MIS 3.

Bioturbated sediments of B2 and the overlying W3 layer are interpreted to represent hemipelagic depositional environments with drifting icebergs during a relatively warm period of MIS 3 (Fig. 7C). In general, Mn-enriched, brown sediments are believed to reflect elevated sea levels and/or reduced sea-ice conditions, under which sediment from the Siberian shelves could be transported to the central Arctic basins (Jakobsson et al., 2000; Polyak et al., 2004, 2009; Stein et al., 2010; Löwemark et al., 2014; Ye et al., 2019). Overall, sedimentary properties of G2 and overlying facies indicate depositional environments affected by the advance and retreat of a marine-based ice sheet grounded on the AP top.

The absence of glaciogenic debris lobe within SSU 1 indicates that the AP has not encountered glacial erosion during MIS 2,



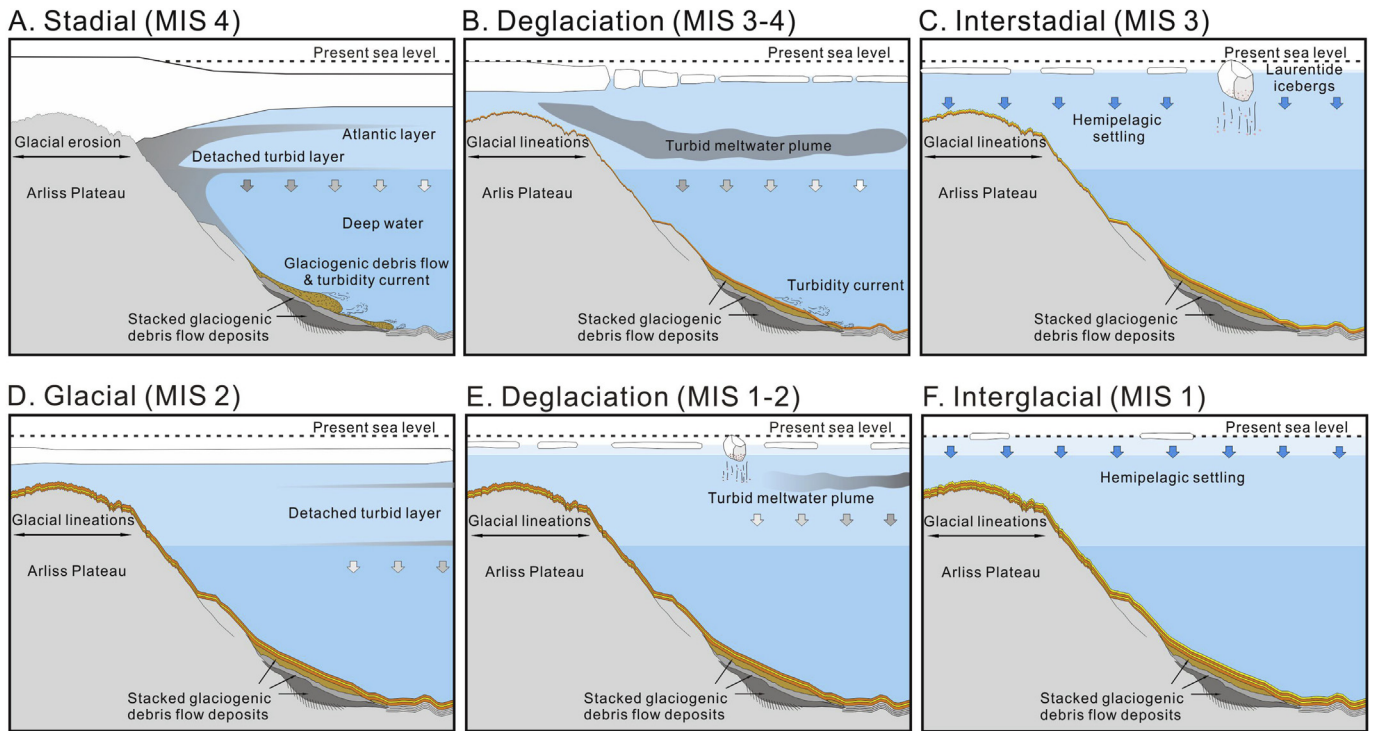


Fig. 7. Schematic model of sedimentary processes on the Arliss Plateau and adjacent Chukchi Basin during major depositional regimes from the MIS 4 glaciation to the Holocene.

consistent with previous studies from the Arctic Ocean off the Siberian margin (Niessen et al., 2013; Schreck et al., 2018) as well as terrestrial studies from adjacent islands and the East Siberian mainland (Romanovskii et al., 2004; Gualtieri et al., 2005). Nevertheless, the presence of CLm facies within unit G1, most of which is attributed to MIS 2 (Figs. 3 and 4), reflects glacier-induced depositional processes, such as the suspension settling of turbid meltwater plumes and detached turbid layers (Fig. 7D and E). This lithology indicates the influence of a limited glaciation in the study region, although its location and distribution pattern (e.g., grounded ice vs. ice shelf) needs to be further investigated. There is no evidence for the LGM glaciation at the East Siberian margin, but data from the eastern Chukchi shelf margin show glaciogenic bedforms indicative of grounded ice, age-constrained to MIS 2 (Polyak et al., 2007). These bedforms are restricted to water depths of less than ~450 m, but we cannot exclude that this grounded ice extended over the Chukchi shelf to its western margin bordering the Chukchi Basin.

The predominance of the bioturbated sandy mud (Bsm) facies in the uppermost unit B1 reflects hemipelagic deposition with sea-ice and/or iceberg debris rafting during much of the Holocene (Fig. 7F). Intense bioturbation indicates a relatively elevated export of primary production to the seafloor, and thus moderate sea-ice conditions, and/or enhanced oxygenation of surface sediments.

## 6. Conclusions

A combination of litho- and seismostratigraphy on the basinward slope of the Arliss Plateau depicts a glacier-induced depositional history in front of the East Siberian continental margin since estimated MIS 5c (~100 ka). The age constraints were obtained by correlation of the studied core ARA02B/16B-GC with earlier developed stratigraphies (Adler et al., 2009; Schreck et al., 2018). Based on this age model and the core-seismic correlation,

deposition of the youngest glaciogenic debris lobes on the slope, indicative of the last glacial erosion of the AP top, occurred within seismostratigraphic unit SSU 2 during MIS 4 to early MIS 3. This event may be correlative to a major glaciation in northern Siberia that has been constrained to the time interval between ~70 and 50 ka (Svendsen et al., 2004; Möller et al., 2015). Laminated sedimentary facies and sedimentation rates as high as ~6 cm/kyr in the respective core interval (lithological unit G2) reflect glacier-induced sediment deposition. This enhanced sedimentation probably resulted from detached turbid layers, turbidity currents, and meltwater discharge pulses during glaciation/deglaciation.

The absence of glaciogenic debris lobes within the upper seismostratigraphic unit SSU 1 (late MIS 3 to 1) indicates that glacial erosion unlikely impacted the AP during the LGM, consistent with previous inferences (Niessen et al., 2013; Schreck et al., 2018). Nevertheless, the presence of laminated facies within the corresponding core interval G1 may indicate a limited glaciation at a nearby continental margin. Further investigation by geophysical seafloor surveys verified by sediment core records is needed to better understand the glacial history of the western Arctic Ocean.

## Acknowledgments

We want to thank the captain and crew of RV Araon for excellent collaboration and support during the 2<sup>nd</sup> Arctic expedition ARA02B in 2011. This research is mainly funded by a seed-type research project (PE19350 to Seung-Il Nam) of Korea Polar Research Institute, Republic of Korea. Leonid Polyak contribution was partially supported by the US National Science Foundation award ARC-1304755, United States. We thank an anonymous reviewer and Matt O'Regan for detailed comments that helped to improve the manuscript.

## References

- Adler, R.E., Polyak, L., Ortiz, J.D., Kaufman, D.S., Channell, J.E.T., Xuan, C., Grotto, A.G., Sellén, E., Crawford, K.A., 2009. Sediment record from the western Arctic Ocean with an improved Late Quaternary age resolution: HOTRAX core HLY0503-8JPC, Mendeleev Ridge. *Glob. Planet. Chang.* 68, 18–29.
- Backman, J., Fornaciari, E., Rio, D., 2009. Biochronology and paleoceanography of late Pleistocene and Holocene calcareous nannofossil abundances across the Arctic Basin. *Mar. Micropaleontol.* 72, 86–98.
- Batchelor, C.L., Dowdeswell, J.A., 2014. The physiography of High Arctic cross-shelf troughs. *Quat. Sci. Rev.* 92, 68–96.
- Batchelor, C.L., Dowdeswell, J.A., 2015. Ice-sheet grounding-zone wedges (GZWs) on high-latitude continental margins. *Mar. Geol.* 363, 65–92.
- Bazhenova, E., Fagel, N., Stein, R., 2017. North American origin of “pink–white” layers at the Mendeleev Ridge (Arctic Ocean): new insights from lead and neodymium isotope composition of detrital sediment component. *Mar. Geol.* 386, 44–55.
- Bischof, J.F., Darby, D.A., 1997. Mid-to Late Pleistocene ice drift in the western Arctic Ocean: evidence for a different circulation in the past. *Science* 277, 74–78.
- Chough, S., 1984. Fine-grained turbidites and associated mass-flow deposits in the ulleung (Tsunami) back-arc basin, east sea (sea of Japan). *Geol. Soc. London Spec. Publ.* 15, 185–196.
- Clark, D.L., Whitman, R.R., Morgan, K.A., Mackey, S.D., 1980. Stratigraphy and Glacial-Marine Sediments of the Amerasian Basin, Central Arctic Ocean. Geological Society of America.
- Cronin, T.M., Dwyer, G.S., Farmer, J., Bauch, H.A., Spielhagen, R.F., Jakobsson, M., Nilsson, J., Briggs Jr., W., Stepanova, A., 2012. Deep Arctic Ocean warming during the last glacial cycle. *Nat. Geosci.* 5, 631.
- Darby, D.A., Bischof, J.F., Jones, G.A., 1997. Radiocarbon chronology of depositional regimes in the western Arctic Ocean. *Deep Sea Res. Part II Top. Stud. Oceanogr.* 44, 1745–1757.
- Dong, L., Liu, Y., Shi, X., Polyak, L., Huang, Y., Fang, X., Liu, J., Zou, J., Wang, K., Sun, F., Wang, X., 2017. Sedimentary record from the Canada Basin, Arctic Ocean: implications for late to middle Pleistocene glacial history. *Clim. Past* 13, 511–531.
- Dove, D., Polyak, L., Coakley, B., 2014. Widespread, multi-source glacial erosion on the Chukchi margin, Arctic Ocean. *Quat. Sci. Rev.* 92, 112–122.
- Dowdeswell, J.A., Elverhøi, A., 2002. The timing of initiation of fast-flowing ice streams during a glacial cycle inferred from glacial marine sedimentation. *Mar. Geol.* 188, 3–14.
- England, J.H., Furze, M.F., Doupé, J.P., 2009. Revision of the NW Laurentide ice sheet: implications for paleoclimate, the northeast extremity of beringia, and Arctic Ocean sedimentation. *Quat. Sci. Rev.* 28, 1573–1596.
- Grobe, H., 1987. A simple method for the determination of ice-rafted debris in sediment cores. *Polarforschung* 57, 123–126.
- Gualtieri, L., Vartanyan, S., Brigham-Grette, J., Anderson, P., 2005. Evidence for an ice-free Wrangel island, northeast Siberia during the last glacial maximum. *Boreas* 34, 264–273.
- Hanslik, D., Jakobsson, M., Backman, J., Björck, S., Sellén, E., O'Regan, M., Fornaciari, E., Skog, G., 2010. Pleistocene Arctic Ocean sea ice and deep water isolation times. *Quat. Sci. Rev.* 29, 3430–3441.
- Hesse, R., Klauke, I., Ryan, W.B., Edwards, M.B., Piper, D.J.W., 1996. Imaging Laurentide ice sheet drainage into the deep sea: impact on sediments and bottom water. *Oceanogr. Lit. Rev.* 4.
- Jakobsson, M., Løvlie, R., Al-Hanbali, H., Arnold, E., Backman, J., Mörth, M., 2000. Manganese and color cycles in Arctic Ocean sediments constrain Pleistocene chronology. *Geology* 28, 23–26.
- Jakobsson, M., Løvlie, R., Arnold, E., Backman, J., Polyak, L., Knutsen, J.-O., Musatov, E., 2001. Pleistocene stratigraphy and paleoenvironmental variation from Lomonosov Ridge sediments, central Arctic Ocean. *Glob. Planet. Chang.* 31, 1–22.
- Jakobsson, M., Grantz, A., Kristoffersen, Y., Macnab, R., 2003. Physiographic provinces of the Arctic Ocean seafloor. *Geol. Soc. Am. Bull.* 115.
- Jakobsson, M., Polyak, L., Edwards, M., Kleman, J., Coakley, B., 2008. Glacial geomorphology of the central Arctic Ocean: the Chukchi borderland and the Lomonosov Ridge. *Earth Surf. Process. Landforms* 33, 526–545.
- Jakobsson, M., Andreassen, K., Bjarnadóttir, L.R., Dove, D., Dowdeswell, J.A., England, J.H., Funder, S., Hogan, K., Ingólfsson, Ó., Jennings, A., Krog Larsen, N., Kirchner, N., Landvik, J.Y., Mayer, L., Mikkelsen, N., Möller, P., Niessen, F., Nilsson, J., O'Regan, M., Polyak, L., Nørgaard-Pedersen, N., Stein, R., 2014. Arctic Ocean glacial history. *Quat. Sci. Rev.* 92, 40–67.
- Jakobsson, M., Nilsson, J., Anderson, L., Backman, J., Björck, G., Cronin, T.M., Kirchner, N., Koshurnikov, A., Mayer, L., Noormets, R., O'Regan, M., Stranne, C., Ananiev, R., Barrientos Macho, N., Cherniykh, D., Coxall, H., Eriksson, B., Flodén, T., Gemery, L., Gustafsson, Ö., Jerram, K., Johansson, C., Khortov, A., Mohammad, R., Semiletov, I., 2016. Evidence for an ice shelf covering the central Arctic Ocean during the penultimate glaciation. *Nat. Commun.* 7, 10365.
- Jokat, W., 2008. The Expedition of the Research Vessel “Polarstern” to the Arctic in 2008 (ARK-XXIII/3).
- Kaufman, D.S., Polyak, L., Adler, R., Channell, J.E., Xuan, C., 2008. Dating Late Quaternary planktonic foraminifer *Neoglobobulimina pachyderma* from the Arctic Ocean using amino acid racemization. *Paleoceanography* 23.
- Kleiber, H., Knies, J., Niessen, F., 2000. The late Weichselian glaciation of the Franz Victoria Trough, northern Barents Sea: ice sheet extent and timing. *Mar. Geol.* 168, 25–44.
- Löwemark, L., O'Regan, M., Hanebuth, T., Jakobsson, M., 2012. Late Quaternary spatial and temporal variability in Arctic deep-sea bioturbation and its relation to Mn cycles. *Paleogeogr. Paleoclimatol. Paleoecol.* 365, 192–208.
- Löwemark, L., März, C., O'Regan, M., Gyllencreutz, R., 2014. Arctic Ocean Mn-stratigraphy: genesis, synthesis and inter-basin correlation. *Quat. Sci. Rev.* 92, 97–111.
- März, C., Stratmann, A., Matthiessen, J., Meinhardt, A.K., Eckert, S., Schnetger, B., Vogt, C., Stein, R., Brumsack, H.J., 2011. Manganese-rich brown layers in Arctic Ocean sediments: composition, formation mechanisms, and diagenetic overprint. *Geochem. Cosmochim. Acta* 75, 7668–7687.
- Matthiessen, J., Niessen, F., Stein, R., Naafs, B.D.A., 2010. Pleistocene glacial marine sedimentary environments at the eastern Mendeleev Ridge, Arctic Ocean. *Polarforschung* 79, 123–137.
- Möller, P., Alexanderson, H., Funder, S., Hjort, C., 2015. The Taimyr Peninsula and the Severnaya Zemlya archipelago, Arctic Russia: a synthesis of glacial history and palaeo-environmental change during the Last Glacial cycle (MIS 5e–2). *Quat. Sci. Rev.* 107, 149–181.
- Niessen, F., Hong, J.K., Hegewald, A., Matthiessen, J., Stein, R., Kim, H., Kim, S., Jensen, L., Jokat, W., Nam, S.-I., 2013. Repeated Pleistocene glaciation of the east Siberian continental margin. *Nat. Geosci.* 6, 842.
- Nørgaard-Pedersen, N., Spielhagen, R.F., Thiede, J., Kassens, H., 1998. Central Arctic surface ocean environment during the past 80,000 years. *Paleoceanography* 13, 193–204.
- O'Regan, M., Backman, J., Barrientos, N., Cronin, T.M., Gemery, L., Kirchner, N., Mayer, L.A., Nilsson, J., Noormets, R., Pearce, C., 2017. The De Long Trough: a newly discovered glacial trough on the East Siberian continental margin. *Clim. Past* 13, 1269.
- ÓCofaigh, C., Taylor, J., Dowdeswell, J.A., Pudsey, C.J., 2003. Palaeo-ice streams, trough mouth fans and high-latitude continental slope sedimentation. *Boreas* 32, 37–55.
- Phillips, L.R., Grantz, A., 1997. Quaternary history of sea ice and paleoclimate in the Amerasia basin, Arctic Ocean, as recorded in the cyclical strata of Northwind Ridge. *Geol. Soc. Am. Bull.* 109, 1101–1115.
- Piper, D.W., 1978. Turbidite muds and silts on deep-sea fans and abyssal plains. In: Stanley, D.J., Kelling, G. (Eds.), *Sedimentation in Submarine Canyons, Fans, and Trenches*, Hutchinson and Ross Stroudsburg, pp. 163–176.
- Poirier, R.K., Cronin, T.M., Briggs Jr., W.M., Lockwood, R., 2012. Central Arctic paleoceanography for the last 50 kyr based on ostracode faunal assemblages. *Mar. Micropaleontol.* 88, 65–76.
- Polyak, L., Curry, W.B., Darby, D.A., Bischof, J., Cronin, T.M., 2004. Contrasting glacial/interglacial regimes in the western Arctic Ocean as exemplified by a sedimentary record from the Mendeleev Ridge. *Paleogeogr. Paleoclimatol. Paleoecol.* 203, 73–93.
- Polyak, L., Darby, D.A., Bischof, J.F., Jakobsson, M., 2007. Stratigraphic constraints on late Pleistocene glacial erosion and deglaciation of the Chukchi margin, Arctic Ocean. *Quat. Res.* 67, 234–245.
- Polyak, L., Bischof, J., Ortiz, J.D., Darby, D.A., Channell, J.E.T., Xuan, C., Kaufman, D.S., Løvlie, R., Schneider, D.A., Eberl, D.D., Adler, R.E., Council, E.A., 2009. Late Quaternary stratigraphy and sedimentation patterns in the western Arctic Ocean. *Glob. Planet. Chang.* 68, 5–17.
- Powell, R.D., 1990. Glacial marine processes at grounding-line fans and their growth to ice-contact deltas. In: Dowdeswell, J.A., Scourse, J.D. (Eds.), *Glacial Marine Environments: Processes and Sediments*, vol. 53. Geological Society of London Special Publication, pp. 53–73.
- Romanovskii, N., Hubberten, H.-W., Gavrillov, A., Tumskey, V., Kholodov, A., 2004. Permafrost of the east Siberian Arctic shelf and coastal lowlands. *Quat. Sci. Rev.* 23, 1359–1369.
- Schreck, M., Nam, S.-I., Polyak, L., Vogt, C., Kong, G.S., Stein, R., Matthiessen, J., Niessen, F., 2018. Improved Pleistocene sediment stratigraphy and paleoenvironmental implications for the western Arctic Ocean off the east Siberian and Chukchi margins. *arXiv:1804.04444*.
- Spielhagen, R.F., Baumann, K.-H., Erlenkeuser, H., Nowaczyk, N.R., Nørgaard-Pedersen, N., Vogt, C., Weiel, D., 2004. Arctic Ocean deep-sea record of northern Eurasian ice sheet history. *Quat. Sci. Rev.* 23, 1455–1483.
- Stein, R., Matthiessen, J., Niessen, F., Krylov, A., Nam, S.-I., Bazhenova, E., 2010. Towards a better (litho-) stratigraphy and reconstruction of Quaternary paleoenvironment in the Amerasian Basin (Arctic Ocean). *Polarforschung* 79, 97–121.
- Stokes, C., Margold, M., Clark, C., Tarasov, L., 2016. Ice stream activity scaled to ice sheet volume during Laurentide Ice Sheet deglaciation. *Nature* 530, 322.
- Svendsen, J., 2004. Late Quaternary ice sheet history of northern Eurasia. *Quat. Sci. Rev.* 23, 1229–1271.
- Thierstein, H., Geitzenauer, K., Molino, B., Shackleton, N., 1977. Global synchronicity of Late Quaternary coccolith datum levels. Validation by oxygen isotopes. *Geology* 5, 400–404.
- Tjallingii, R., Röhl, U., Kölling, M., Bickert, T., 2007. Influence of the water content on X-ray fluorescence core-scanning measurements in soft marine sediments. *Geochem. Geophys. Geosyst.* 8 (2) <https://doi.org/10.1029/2006GC001393>.
- Vorren, T.O., Laberg, J.S., B. F., Dowdeswell, J.A., K. N.H., M. J., R. J., Werner, F., 1998. The Norwegian-Greenland sea continental margins: morphology and Late Quaternary sedimentary processes and environment. *Quat. Sci. Rev.* 17, 273–302.
- Wang, R., Xiao, W., März, C., Li, Q., 2013. Late Quaternary paleoenvironmental changes revealed by multi-proxy records from the Chukchi abyssal plain, western Arctic Ocean. *Glob. Planet. Chang.* 108, 100–118.
- Wang, R., Polyak, L., Xiao, W., Wu, L., Zhang, T., Sun, Y., Xu, X., 2018. Late-Middle

- Quaternary lithostratigraphy and sedimentation patterns on the Alpha Ridge, central Arctic Ocean: implications for Arctic climate variability on orbital time scales. *Quat. Sci. Rev.* 181, 93–108.
- Ye, L., März, C., Polyak, L., Yu, X., Zhang, W., 2019. Dynamics of manganese and cerium enrichments in Arctic Ocean sediments: a case study from the Alpha Ridge. *Front. Earth Sci.* 6.
- Yoon, S., Chough, S., Thiede, J., Werner, F., 1991. Late Pleistocene sedimentation on the Norwegian continental slope between 67 and 71 N. *Mar. Geol.* 99, 187–207.